

Composite Luminosity Functions based on the Sloan Digital Sky Survey “Cut and Enhance” Galaxy Cluster Catalog

Tomotsugu GOTO^{1,2,3}, Sadanori OKAMURA⁴, Timothy A. MCKAY⁵,
Neta A. BAHCALL⁶, James ANNIS⁷, Mariangela BERNARDI²,
J. BRINKMANN⁸, Percy L. GÓMEZ², Sarah HANSEN⁵,
Rita S. J. KIM⁹, Maki SEKIGUCHI¹ and Ravi K. SHETH¹⁰

¹*Institute for Cosmic Ray Research, University of Tokyo,
Kashiwanoha, Kashiwa, Chiba 277-0882, Japan*

²*Department of Physics, Carnegie Mellon University,
5000 Forbes Avenue, Pittsburgh, PA 15213-3890, USA*

³*tomo@cmu.edu*

⁴*Department of Astronomy and Research Center for the Early Universe,
School of Science, University of Tokyo, Tokyo 113-0033, Japan*

⁵*University of Michigan, Department of Physics,
500 East University, Ann Arbor, MI 48109, USA*

⁶*Princeton University Observatory, Princeton, NJ 08544, USA*

⁷*Fermi National Accelerator Laboratory, P.O. Box 500, Batavia, IL 60510, USA*

⁸*Apache Point Observatory,*

2001 Apache Point Road, P.O. Box 59, Sunspot, NM 88349-0059, USA

⁹*Department of Physics and Astronomy, The Johns Hopkins University,
3400 North Charles Street, Baltimore, MD 21218-2686, USA*

¹⁰*Department of Physics and Astronomy University of Pittsburgh
3941 O’Hara Street Pittsburgh, PA 15260*

(Received 2002 April 9; accepted 2002 May 15)

Abstract

We present here results on the composite luminosity functions (LF) of galaxies in the clusters of galaxies selected from the Cut and Enhance cluster catalog (CE) of the Sloan Digital Sky Survey. We constructed composite LFs in the five SDSS bands, u, g, r, i and z , using 204 CE clusters ranging from $z = 0.02$ to $z = 0.25$. Background and foreground galaxies were subtracted from the LF using an annular region around clusters to take large-scale, galaxy-number-count variances into consideration. A LF of each cluster was weighted according to the richness and number of contributing galaxies to construct the composite LF. Taking advantage of accurate

photometry of SDSS, we used photometric redshifts to construct composite luminosity functions and thus study a large number of clusters. The robustness of the weighting scheme was tested using a Monte-Carlo simulation. The best-fit Schechter parameters are $(M^*, \alpha) = (-21.61 \pm 0.26, -1.40 \pm 0.11), (-22.01 \pm 0.11, -1.00 \pm 0.06), (-22.21 \pm 0.05, -0.85 \pm 0.03), (-22.31 \pm 0.08, -0.70 \pm 0.05)$ and $(-21.36 \pm 0.06, -0.58 \pm 0.04)$ in u, g, r, i and z , respectively. We find that the slope of composite LFs becomes flatter toward a redder color band. Compared with the field LFs of the SDSS, the cluster LFs have brighter characteristic magnitude and flatter slopes in the g, r, i and z bands. These results are consistent with the hypothesis that the cluster LF has two distinct underlying populations i.e. the bright end of the LF is dominated by bright early types that follow a Gaussian-like luminosity distribution, while the faint-end of the cluster LF is a steep power-law like function dominated by star-forming (bluer) galaxies. We also studied the composite LFs for early-type and late-type galaxies using profile fits, a concentration parameter and $u - r$ color to classify galaxy morphology. A strong dependence of LF on galaxy morphology was found. The faint end slope of the LF is always flatter for early-type galaxies than late-type, regardless of the passband and methodology. These results are consistent with the hypothesis that the cluster regions are dominated by bright elliptical galaxies. This work also provides a good low-redshift benchmark for on-going multi-color photometric studies of high redshift clusters of galaxies using 4–8 m class telescopes.

Key words: galaxies: luminosity function, mass function — galaxies: clusters: general — galaxies : fundamental parameters

1. Introduction

The luminosity function (LF) of galaxies within clusters of galaxies is a key tool for understanding the role of the environment on galaxy formation and evolution. The shape of the cluster LF as a function of the galaxy colors and morphologies, as well as a function of the cluster radius or local density, can provide strong observational constraints on the theories of galaxy formation. For example, Springel et al. (2001) recently showed that semi-analytical models of hierarchical structure formation could now explain both the shape of the composite cluster LF (B -band LF of Trentham 1998) and the morphology-radius relationship of Whitmore et al. (1993) using just a simple prescription for the properties of galaxies in clusters based on their merger and cooling rates (see also Okamoto, Nagashima 2001). Empirically, there is also growing evidence for a correlation between the shape of the cluster LF and the underlying cluster properties. Phillipps et al. (1998) and Driver et al. (1998) show that more evolved clusters, based on either their density profile or the presence of a cD galaxy, have flatter faint-end slopes, which they attribute to the disruption of faint galaxies in the cores of such

evolved systems [see the earlier theoretical work on galaxy cannibalism by Hausman & Ostriker (1978)]. In summary, the LF of galaxies in clusters as a function of both the galaxy and cluster properties is a powerful observational test for theories of galaxy formation and evolution. The reader is referred to the seminal review by Binggeli, Sandage, and Tammann (1988), which is still relevant today.

In this paper, we present an analysis of the composite cluster LF based on the commissioning data of the Sloan Digital Sky Survey (SDSS; see Gunn et al. 1998; York et al. 2000; Stoughton et al. 2002). This analysis has several key advantages over previous studies of the composite cluster LF, including accurate multi-color CCD photometry for all galaxies (in optical passbands u, g, r, i and z ; Fukugita et al. 1996), large aerial coverage, thus enabling us to make a local correction for the projected field LF, and finally, the availability of several objectively-measured galaxy properties like morphology. Furthermore, we selected our clusters from the SDSS Cut and Enhance (CE) cluster catalog of Goto et al. (2002), which has two major benefits over previous cluster samples used for LF studies. First, the CE catalog was objectively constructed using the latest cluster-finding algorithms, and therefore has a well-determined selection function (see Goto et al. 2002). Secondly, CE has obtained an accurate photometric redshift for each cluster based on the observed color of the E/S0 ridge-line using the method of J. Annis et al. (in preparation). The error on this cluster photometric redshift is only $\delta z = 0.015$ for $z < 0.3$ clusters (see figure. 14 of Goto et al. 2002) and, as we show herein, is accurate enough to allow us to determine the composite LF for a large sample of CE clusters without the need for spectroscopic redshifts. Thus, our analysis of the composite cluster LF is based on one of the largest sample of clusters to date.

We present this work now to provide a low-redshift benchmark for on-going multi-color photometric studies of high redshift clusters of galaxies. With the advent of large-area CCD imagers on large telescopes, the number of distant clusters with such data will increase rapidly over the next few years; e.g. Kodama et al. (2001) recently presented large-area multi-color CCD photometry for the distant cluster A 851 ($z = 0.41$) using Suprime-Cam on the Subaru Telescope. Gladders and Yee. (2000) searched distant clusters over 100 deg^2 of CCD data. This paper is organized as follows: In section 2 we describe the methods used to construct the composite LF of CE clusters and show our results as a function of passband and morphology. In section 3 we test the robustness of the analysis, and in section 4 we summarize our work. Throughout this paper, we use $h_0 = 0.7$, $\Omega_M = 0.3$ and $\Omega_\Lambda = 0.7$.

2. SDSS Data

In this section, we outline the data used in this paper. The photometric data used herein was taken from the SDSS commissioning data, as discussed by York et al. (2000). Our analysis focuses on the 150 deg^2 contiguous area made up from the overlap of SDSS photometric runs 752 & 756 i.e. $145.^\circ 1 < \text{R.A.} < 236.^\circ 1$ and $-1.^\circ 25 < \text{Dec.} < +1.^\circ 25$. This is a subset of the SDSS Early

Data Release, as discussed in Stoughton et al. (2002), and similar to the data used by Scranton et al. (2002) for studying the angular clustering of SDSS galaxies. This photometric data reach 5σ detection limits for point sources of 22.3, 23.3, 23.1, 22.3 and 20.8 mag in the u, g, r, i and z passbands, respectively (for an airmass of 1.4 and $1''$ seeing)¹. The photometric uniformity of the data across the whole area is less than 3% [see Hogg et al. (2001) and Smith et al. (2002) for photometric calibration], while the star-galaxy separation is robust to $r \simeq 21.0$ (Scranton et al. 2002). This is significantly better than previous photographic surveys, which suffer from larger plate-to-plate photometric fluctuations and a lower dynamic range [see Lumsden et al. 1997 for the problems associated with photographic studies of the cluster composite LF]. For each galaxy, we used the model magnitude computed by the PHOTO data analysis pipeline, which has been shown by Lupton et al. (2001) and Stoughton et al. (2002) to be the optimal magnitude for faint SDSS galaxies. It is also close to the total magnitude for the fainter SDSS galaxies. For a full discussion of the photometric data, and the galaxy parameters derived from that data, we refer the reader to Lupton et al. (2001) and Stoughton et al. (2002).

The clusters used herein were drawn from the large sample of CE clusters presented in Goto et al. (2002), which were selected over the same photometric runs of 752 & 756. We only selected the richer systems which were determined by the number of galaxies brighter than -18 th magnitude, (N_{-18}). The CE clusters used here satisfy the following conditions:

- 1) Number of galaxies brighter than -18 th magnitude in the r band (N_{-18}) > 20 ,
- 2) $0.02 < z < 0.25$.

Condition 1 was used to select richer systems. N_{-18} is defined as the number of galaxies brighter than -18 th magnitude in the r band after subtracting the background using the method described in section 3 to construct composite LFs. Galaxies within 0.75 Mpc from a cluster center were used. Condition 1 was used to avoid letting small groups with only a few very bright galaxies dominate the composite LFs in the weighting scheme. (The weighting scheme is explained in detail in section 3.) Even though we used $N_{-18} > 20$ as a criteria to select our clusters, we show in section 4 that our composite LFs were not affected by this richness criteria. Since the high redshift clusters ($z \sim 0.3$) are not imaged to the fainter galaxies, we restricted our clusters to be in the range $0.02 < z < 0.25$. In total, 204 clusters satisfy these criteria.

3. Analysis and Results

3.1. Construction of the Composite Cluster LF

We discuss here the construction of the composite luminosity function of galaxies within the subsample of the CE clusters discussed above. The first critical step in such an analysis is

¹ The photometry obtained at this early stage of SDSS is denoted u^*, g^*, r^*, i^* , and z^* to stress the preliminary nature of the calibration.

the subtracting the background and foreground contamination. Ideally, one would wish to do this via spectroscopic observations, but since the CE cluster catalog contains ~ 2000 galaxies in the region used, it is not feasible to observe all clusters spectroscopically. Therefore, we must make a statistical correction based on the expected contamination from projected field galaxies. One of the main advantages of the SDSS data is that such a correction can be estimated locally (i.e. free from any galaxy number count variances due to the large-scale structure) for each cluster since we possess all the photometric data, to the same depth and in the same filter set, well outside of the cluster. Indeed, such local background subtraction was thought to be ideal in previous works, but was not possible due to the small coverage of the sky.

For the composite cluster LF, we only used galaxies within 0.75 Mpc of the cluster centroid. This radius was determined empirically so as not to lose statistics by using a too small radius, and not to lose the contrast of clusters against the background by using a too large radius. Foreground and background contamination were corrected for using an annulus around each cluster with an inner radius of 1.5 Mpc and an outer radius of 1.68 Mpc. These radii represent a compromise between having as large an aperture as possible to avoid removing legitimate cluster galaxies, while still providing an accurate estimate of the local projected field population. Since the background/foreground galaxies are themselves highly clustered, it is important to obtain as local an estimate as possible. The photometric redshift of each cluster was used to convert these metric apertures into angular apertures. The center of each cluster was taken from the CE catalog, and estimated from the position of the peak in the enhanced density map of Goto et al. (2002). The cluster centroids were expected to be determined with an accuracy better than ~ 40 arcsec through Monte-Carlo simulation. When an annulus touches the boundary of the SDSS data, we corrected for contamination using the number-magnitude relationship of the whole data set instead (this only affected a few of the clusters used herein).

Since each sample cluster has a different redshift, each cluster reaches the SDSS apparent magnitude limit at different absolute magnitudes. Also, because they have various richnesses, the number of galaxies in each cluster is different. To take these different degrees of completeness into account, we followed the methodology of Colless (1989) to construct the composite cluster LF. The individual cluster LFs are weighted according to the cluster richness and the number of clusters which contribute to a given bin. This is written as

$$N_{cj} = \frac{m_j}{N_{c0}} \sum_i \frac{N_{ij}}{N_{i0}}, \quad (1)$$

where N_{cj} is the number of galaxies in the j th bin of the composite LF, N_{ij} is the number in the j th bin of the i th cluster LF, N_{i0} is the normalization of the i th cluster LF, and was measured to be the field-corrected number of galaxies brighter than $M_{r^*} = -18$, m_j is the number of clusters contributing the j th bin and, finally, $N_{c0} = \sum_i N_{i0}$. The formal errors on the composite LF were computed using

$$\delta N_{cj} = \frac{N_{c0}}{m_j} \left[\sum_i \left(\frac{\delta N_{ij}}{N_{i0}} \right)^2 \right]^{1/2}, \quad (2)$$

where δN_{cj} and δN_{ij} are the errors on the j th bin for the composite and i th cluster, respectively. In this way we can take into account the different degrees of completeness.

Like other authors, we discarded the Brightest Cluster Galaxy (BCG) within 0.75 Mpc of the cluster centroid when constructing the composite LF, since such BCGs tend not to follow the cluster LF. We only used SDSS galaxies brighter than $r^*=21.0$, since this is the limit of the SDSS star–galaxy separation (Scranton et al. 2002; Lupton et al. 2001). This magnitude limit and weighting scheme combined with our cosmology enabled us to dig LF down to $M_{r^*}=-17.5$. When converting apparent to absolute magnitudes, we assumed a k-correction for the early-type galaxy given by Fukugita et al. (1995).

In figure 1, we show the composite LF of the subset of CE clusters discussed above. We present one composite LF for each of the five SDSS passbands. We also present in table 1 the best-fit parameters from a joint fit of a Schechter function to these data. For a comparison, we also show the field values as derived by Blanton et al. (2001) (corrected for $h_0 = 0.7$). In figure 1, field LFs normalized to cluster LFs are shown by dotted lines. As expected, the M^* for our cluster LFs is significantly brighter (by 1 – 1.5 magnitudes depending on the bands) than those seen for the field LFs in all five bands. Furthermore, the faint end slopes (α) of the cluster composite LFs are much flatter than those seen for the field LFs. This is especially noticeable for the redder passbands (i and z) while the slope of the cluster LF systematically flattens from the u passband to the z passband.

These results are consistent with the hypothesis that the cluster LF has two distinct underlying populations i.e. the bright end of the LF is dominated by bright early types that follow a Gaussian-like luminosity distribution, while the faint-end of the cluster LF is a steep power-law-like function dominated by star-forming (bluer) galaxies. Binggeli et al. (1988) originally suggested this hypothesis, while the recent work of Adami et al. (2000), Rakos et al. (2000) and Dressler et al. 1999 supported this idea. Particularly, Boyce et al. (2001) showed LF of Abell 868 is made up of three different populations of galaxies; luminous red and two fainter blue populations. The idea is illustrated by the fact that the cluster LFs in the redder passbands, which are presumably dominated by the old stellar populations of the early types, have much brighter M^* 's and significantly shallower slopes than those measured in the bluer passbands. Those results can also be interpreted as showing that bright elliptical galaxies are more populated in dense regions, like inside of clusters. They are consistent with the morphology-density relation advocated by Dressler et al. (1980, 1997).

3.2. The Composite Cluster LF as a Function of Morphology

One of the key aspects of the SDSS photometric data is the opportunity to statistically study the distribution of galaxies as a function of their morphology. In this subsection,

we discuss the composite cluster LF as a function of morphology using three complementary methods for determining the morphological type of each galaxy. These include: i) the best-fit de Vaucouleur or exponential model profile; ii) the inverse of concentration index and iii) the $u - r$ color of the galaxies. We present all three methods, since at present it is unclear which method is the most successful at separating the different morphological galaxy types. Also, each method suffers from different levels of contamination, and the differences in the methods can be used to gauge the possible systematic uncertainties in the morphological classifications. We discuss the three methods used in detail below.

The first method we consider here is using the de Vaucouleur and exponential model fits of the galaxy light profiles measured by SDSS photometric pipeline (*PHOTO* R.H. Lupton et al., in preparation) to broadly separate galaxies into the late and early-type. If the likelihood of a de Vaucouleur model fit to the data is higher than the that of an exponential model fit, the galaxy is called a late-type, and vice versa. Galaxies that have the same likelihoods for both model fits are discarded. In figure 2, we present the composite cluster LF of late-type and early-type galaxies (as defined using the model fits above) for all five SDSS passbands. In table 2, we present the best-fit Schechter function parameters to these data, and show the fits in figure 2.

The second method uses the inverse of the concentration index, which is defined as $C = r_{50}/r_{90}$, where r_{50} is the radius that contains 50% of the Petrosian flux and r_{90} is the radius that contains 90% of the Petrosian flux (see R.H. Lupton et al., in preparation). Both of these parameters are measured by the SDSS PHOTO analysis pipeline for each galaxy. The concentration parameter used here (C) is just the inverse of the commonly used concentration parameter, and thus early-type galaxies have a lower C parameter than late-type galaxies. The correlation of C with visually-classified morphologies has been studied in detail by Shimasaku et al. (2001) and Strateva et al. (2001). They found that galaxies with $C < 0.4$ are regarded as early-type galaxies, while galaxies with $C \geq 0.4$ are regarded as late-type galaxies. Therefore, in figure 3, we show the composite cluster LF of late-type and early-type galaxies as defined using this second method for all five SDSS passbands. In table 3, we present the best-fit Schechter function parameters to these data.

The third method used herein for morphological classification was to use the observed $u - r$ color of the galaxy which has been proposed by Strateva et al. (2001). Using the fact that k-correction for $u - r$ is almost constant until $z = 0.4$, they showed that galaxies shows a clear bimodal distribution in their $u - r$ color and $u - r = 2.2$ serves as a good classifier of morphology until $z \sim 0.4$ by correlating $u - r$ classification with visual classifications. Therefore, we have classified galaxies with $u - r < 2.2$ as early-type and galaxies with $u - r \geq 2.2$ as late-type. Figure 4 shows the composite cluster LF for both types of galaxies along with their best-fit Schechter functions (in all five passbands). The best-fit Schechter parameters are summarized in table 4.

As expected, there are noticeable differences in these three morphological classifications, as portrayed by the differences in their composite LFs (see figures. 2, 3, and 4). However, it is worth stressing here the similarities between the methods. For example, the faint end slope of the LF is always shallower for early-type galaxies than late-type, regardless of the passband and methodology. Also, the faint end slope for early-type galaxies decreases steadily toward the redder passbands, while the faint-end slope for the late-type galaxies is nearly always above -1 and consistent (or steeper) than the field LF in most passbands. These observations are again qualitatively in agreement with the hypothesis that the bright end of the cluster LF is dominated by bright, old early-types, while the faint-end of the cluster LF represents late-type galaxies maybe in greater numbers than the average field. This model is in agreement with hierarchical models of structure formation and the model for the tidal disruption of dwarf galaxies by the dominant early types.

4. Discussion

In this section, we discuss various tests which we have performed on our measurement and results.

4.1. Monte-Carlo Simulations

To test the robustness of our methods, we performed Monte-Carlo simulations which involved adding artificial clusters to the SDSS data and computing their composite LF using the same algorithms and software as used on the real data. Our model for the artificial clusters was constructed using the SDSS data on Abell 1577 (at $z \sim 0.14$, richness ~ 1). We used the method described in Goto et al. (2002) to make artificial clusters. The radial profile for the artificial clusters was taken to be a King profile (Ichikawa 1986) with a concentration index of 1.5 and a cut-off radius of 1.4 Mpc, which is the size of Abell 1577 (Struble, Rood 1987). The color-magnitude distributions for the artificial clusters were set to be the observed, field-corrected, color-magnitude distributions of Abell 1577 binned into 0.2 magnitude bins in both color and magnitude. From this model, we then constructed artificial clusters as a function of the redshift and overall richness. For redshift, we created clusters at $z = 0.2, 0.3, 0.4$ and 0.5 , ensuring that we properly accounted for the cosmological effects; i.e. the clusters became smaller, redder and dimmer with redshift. We used the k-corrections for an early type spectrum. For richness, we change the number of galaxies within each cluster randomly between 10 and 50. For each redshift, we created 100 clusters (400 clusters in total). The galaxies within these artificial cluster were distributed randomly in accordance with the radial and color-magnitude distributions discussed above. We made no attempt to simulate the density-morphology relation nor the luminosity segregation in clusters.

The artificial clusters were randomly distributed within the real SDSS imaging data and we constructed a composite LF for these clusters using exactly the same software as for the

real clusters. Since the artificial clusters were all made from the same luminosity distribution, the composite LF should therefore look very similar in shape as the original input LF. Figure 5 shows the result of our Monte-Carlo simulations. The histogram shows the original absolute magnitude distribution of Abell 1577 after a field correction, while the symbols show the composite luminosity functions which we constructed as a function of the input redshift.

4.2. Check of Photometric Redshifts

One of the most innovative parts of this analysis is the use of photometric redshifts to determine the composite luminosity function of clusters. As demonstrated in Goto et al. (2002), the accuracy of photometric redshift is excellent ($\delta z = \pm 0.015$ for $z < 0.3$) and this method will certainly be used in the near future as the number of clusters with photometric redshifts will increase rapidly, far quicker than the number of clusters with spectroscopically confirmed redshifts.

To justify our use of photometric redshifts, since all previous composite cluster LF's used spectroscopic redshifts, we constructed a composite LF using only the clusters with spectroscopically confirmed redshifts. We derived our spectroscopic redshift for CE clusters by matching the SDSS spectroscopic galaxy data with our CE clusters. This was achieved by searching the SDSS spectroscopic galaxy sample for any galaxies within the CE cluster radius and within $\delta z = \pm 0.01$ of the photometric redshift of the cluster. The radius used here was from Goto et al. (2002). If multiple galaxies satisfied this criteria, the closest spectroscopic redshift to the photometric redshift was adopted. The number of clusters with spectroscopic redshifts was 75 out of 204 at the date of this writing.

The results of this test are shown in figure 1 (in the bottom right-hand panel). Also the parameters for the best-fit Schechter functions are given in table 1. and referred to as $r^*(\text{spec})$. We only performed this test for the r passband. The slope and characteristic magnitude of the best-fit Schechter function for the spectroscopically determined LF is in good agreement with that derived using photometric redshifts. As can be seen in table 1, both M_r^* and the slope agree within the error. This test shows that we can truly construct composite LFs using photometric redshift of clusters.

4.3. Test of Cluster Centroids

One key aspect of measuring the composite cluster LF is the choice of the cluster centroid. To test the effect of different cluster centroids on the composite LF, we constructed a composite cluster LF using the position of Brightest Cluster Galaxies (BCGs) as a centroid instead of the peak in the enhanced density map, as discussed in Goto et al. (2002). The BCGs have been determined to be the brightest galaxy among galaxies fainter than -24 th magnitude within 0.75 Mpc. Galaxies brighter than -24 th magnitude are regarded as being foreground galaxies. The mean offset between the BCG position and the centroid previously used is 1.02 arcmin. Table 5 lists the parameters of the best-fit Schechter functions to the five SDSS passbands,

which should be compared to the values obtained using the optical centroid given in table 1. In all five bands, the characteristic magnitudes and slopes agree very well within the error. This test shows that our composite LFs are not dependent on a center determination.

4.4. *Test of Background Subtraction*

Since we constructed composite LFs from 2-dimensional, projected sky image, subtraction of fore/background galaxies played an important role in this work. We test here the effect of making a global background subtraction for all clusters instead of the local background subtraction discussed above. We use the number-magnitude relation of all the galaxies in the entire 150 deg² region as the global background. Table 6 gives the best-fit Schechter parameters of composite LFs constructed using global background subtraction. Compared with table 1, again, every Schechter parameter agrees very well within 1 σ . Although we use annuli around clusters to subtract the background to avoid the large-scale structure disturbing the measurement of composite LFs, this test shows that our composite LFs are not dependent on background subtraction. Valotto et al. (2001) showed that a statistical background subtraction can not re-produce composite LFs using a mock galaxy catalog constructed from a large N -body simulation. Our result, however, combined with the fact that we derived the same LF as input through a Monte-Carlos simulation (in subsection 4.1), supports that our composite LFs are not subject to background subtraction.

4.5. *Test of Cluster Richness*

Another aspect we were concerned about was our choice of cluster richness criteria. To test this, we constructed composite LFs of different subsample with $N_{-18} > 20$ and $N_{-18} > 40$, given in table 7. N_{-18} here is defined as the number of galaxies brighter than -18 th magnitude after subtracting the background in the way we construct composite LFs. $N_{-18} > 20$ was used to construct composite LFs, as mentioned in section 3. In table 7, even though M^* is slightly brighter and the slope is slightly steeper for the richer sample, they agree within 1 σ . The steepening of the slopes can be interpreted as a bias in selecting richer systems using N_{-18} , i.e. Clusters with steeper tails tend to have a larger value of N_{-18} . This, however, confirms that our composite LFs are not dependent on the richness criteria, which we chose.

4.6. *Comparison with Other LFs*

As the final test of our composite cluster LF, we compare here our composite LFs with previous works. First, we must be careful to match the different cosmologies used by various authors as well as the different photometric passbands. To facilitate such a comparison, therefore, we present in table 8 the best-fit Schechter function parameters for our composite LF, but calculated for each author's cosmology and passband using the color corrections of Fukugita et al. (1995) and Lumsden et al. (1992).

In the case of the three b_j photographic surveys of Colless (1989), Valotto et al. (1997),

and Lumsden et al. (1997), we find a significantly brighter M^* than these studies as well as a much shallower slope. We also tried to fit a Schechter function using their α value for the slope, but M^* 's become even brighter. The fits are not good when fixed α 's are used.

Lugger (1989) found $M_R = -22.81 \pm 0.13$ and $\alpha = -1.21 \pm 0.09$ by re-analyzing nine clusters presented in Lugger (1986). The slope is steeper and M^* is slightly brighter than our results. When we fix the slope with her value at $\alpha = -1.21$, the two LFs agree well.

Garilli et al. (1999) studied 65 Abell and X-ray selected samples of galaxies in the magnitude range of $-23.0 < M_r < -17.5$ and found that $M_r^* = -22.16 \pm 0.15$ and $\alpha = -0.95 \pm 0.07$ (in isophotal magnitudes). This slope is steeper than ours. A possible difference with ours is that they used the color condition to select cluster galaxies. M^* is in agreement with our results within the error. We also tried to fit a Schechter function with a fixed value of $\alpha = 0.84$. M^* became brighter by 0.18 mag although the fit was poor.

Paolillo et al. (2001) studied composite LF of 39 Abell clusters using the digitized POSS-II plates. They obtained $M^* = -22.17 \pm 0.16$ in r . The slope is $\alpha = -1.11_{-0.09}^{+0.07}$. Although the slope differs significantly, M^* agrees well compared with our composite LF.

Yagi et al. (2002a,b) observed 10 nearby clusters with their Mosaic CCD camera to derive composite LF. Their best-fit Schechter parameters are $M^* = -21.1 \pm 0.2$ and $\alpha = -1.49 \pm 0.05$ in R . They also studied type-specific LF using exponential and $r^{1/4}$ profile fits to classify the galaxy types. They derived $M^* = -21.1$ and $\alpha = -1.49$ for exponential galaxies and $M^* = -21.2$ and $\alpha = -1.08$ for $r^{1/4}$ galaxies. Considering that they derived composite LFs using the data taken with different instruments analyzed in a different way, it is reassuring that they reached the same conclusion as our results discussed in subsection 3.2. i.e. exponential galaxies have the steeper faint end tail than $r^{1/4}$ galaxies, while their M^* are almost the same.

Concerning the disagreement of our LFs with previous studies, various differences in measuring composite LFs may be the reason. The possible sources of differences are different ways of weighting, different ways of background subtraction, and different depths of the luminosity function. The sample clusters, themselves, should have, to some extent, different richness distributions. For M^* , although we tried to transform our magnitude into their magnitude, the color conversion between SDSS bands and others might not be accurate enough. Thus, the difference with the previous studies is not necessarily a mistake in the analysis, but rather it represents a different way of analysis. Throughout our analysis discussed in section 3 we carefully used exactly the same way to construct the composite LFs. We thus keep our composite LFs internally consistent.

5. Conclusions

We studied the composite LF of 204 the SDSS CE galaxy clusters. The over-all composite LF is compared with other composite LFs. Comparing it to the field luminosity function, a tendency of a brighter M^* and a flatter slope is seen. This is consistent with our understanding

that cluster regions are dominated by brighter galaxies than field galaxies. We divided the composite LF by galaxy morphology in three ways. In all three cases, we found that early-type galaxies have flatter slopes than late-type galaxies. These observations are in agreement with the hypothesis that the bright end of the cluster LF is dominated by bright, old early-types, while the faint-end of the cluster LF represents late-type galaxies. This is also consistent with the morphology–density relation originally advocated by Dressler et al. (1980, 1997). We also studied these composite LFs in five SDSS color bands. The slopes become flatter and flatter toward the redder color bands. This again suggests that cluster regions are dominated by elliptical galaxies with old stellar population. These composite LFs provide a good low redshift benchmark to study higher-redshift clusters in the future. Since the data used in this work came from 2% of the SDSS data, further studies with large SDSS data will increase the statistical significance on these topics as the SDSS proceeds.

We would like to thank the referee, Steven Phillipps, for a detailed revision and useful recommendations provided for this work. We are grateful to Michael Crouch and Christopher J. Miller for valuable comments, which contributed to improve the paper. T.G. wishes to thank Robert C. Nichol for hospitality during the stay at Carnegie Mellon University. T. G. acknowledges financial support from the Japan Society for the Promotion of Science (JSPS) through JSPS Research Fellowships for Young Scientists.

The Sloan Digital Sky Survey (SDSS) is a joint project of The University of Chicago, Fermilab, the Institute for Advanced Study, the Japan Participation Group, the Johns Hopkins University, the Max-Planck-Institute for Astronomy, New Mexico State University, Princeton University, the United States Naval Observatory, and the University of Washington. Apache Point Observatory, site of the SDSS telescopes, is operated by the Astrophysical Research Consortium (ARC). Funding for the project has been provided by the Alfred P. Sloan Foundation, the SDSS member institutions, the National Aeronautics and Space Administration, the National Science Foundation, the U. S. Department of Energy, Japanese Monbukagakusho, and the Max Planck Society. The SDSS Web site is <http://www.sdss.org/>.

References

- Adami, C., Ulmer, M. P., Durret, F., Nichol, R. C., Mazure, A., Holden, B. P., Romer, A. K., & Savine, C. 2000, *A&A*, 353, 930
- Binggeli, B., Sandage, A., & Tammann, G. A. 1988, *ARA&A*, 26, 509
- Blanton, M. R., Dalcanton, J., Eisenstein, D., Loveday, J., Strauss, M. A., SubbaRao, M., Weinberg, D. H., Anderson, J. E., et al. 2001, *AJ*, 121, 2358
- Boyce, P. J., Phillipps, S., Jones, J. B., Driver, S. P., Smith, R. M., & Couch, W. J. 2001, *MNRAS*, 328, 277.
- Colless, M. 1989, *MNRAS*, 237, 799

- Dressler, A. 1980, *ApJ*, 236, 351
- Dressler, A., Oemler, A. J., Couch, W. J., Smail, I., Ellis, R. S., Barger, A., Butcher, H., Poggianti, B. M., & Sharples, R. M., et al. 1997, *ApJ*, 490, 577
- Dressler, A., Smail, I., Poggianti, B. M., Butcher, H., Couch, W. J., Ellis, R. S., & Oemler, A. J. 1999, *ApJS*, 122, 51
- Driver, S. P., Couch, W. J., & Phillipps, S. 1998, *MNRAS*, 301, 369
- Fukugita, M., Shimasaku, K., & Ichikawa, T. 1995, *PASP*, 107, 945
- Fukugita, M., Ichikawa, T., Gunn, J. E., Doi, M., Shimasaku, K., & Schneider, D. P. 1996, *AJ*, 111, 1748.
- Garilli, B., Maccagni, D., & Andreon, S. 1999, *A&A*, 342, 408
- Gladders, M. D., & Yee, H. K. C. 2000, *AJ*, 120, 2148
- Goto, T., Sekiguchi, M., Nichol, R. C., Bahcall, N. A., Kim, R. S. J., Annis, J., Ivezić, Željko, Brinkmann, J., et al. 2002, *AJ*, 123, 1807
- Gunn, J. E., Carr, M., Rockosi, C., Sekiguchi, M., Berry, K., Elms, B., de Haas, E., Ivezić, Ž., et al. 1998, *AJ*, 116, 3040
- Hausman, M. A., & Ostriker, J. P. 1978, *ApJ*, 224, 320
- Heydon-Dumbleton, N. H., Collins, C. A., & MacGillivray, H. T. 1989, *MNRAS*, 238, 379
- Hogg, D. W., Finkbeiner, D. P., Schlegel, D. J., & Gunn, J. E. 2001, *AJ*, 122, 2129
- Ichikawa, S. 1986, *Ann. Tokyo Astron. Obs.*, 21, 77
- Kodama, T., Smail, I., Nakata, F., Okamura, S., & Bower, R. G. 2001, *ApJ*, 562, L9
- Lugger, P. M. 1986, *ApJ*, 303, 535
- Lugger, P. M. 1989, *ApJ*, 343, 572.
- Lumsden, S. L., Collins, C. A., Nichol, R. C., Eke, V. R., Guzzo, L., 1997, *MNRAS*, 290, 119
- Lumsden, S. L., Nichol, R. C., Collins, C. A., & Guzzo, L. 1992, *MNRAS*, 258, 1
- Lupton, R. H., Gunn, J. E., Ivezić, Z., Knapp, G. R., Kent, S., & Yasuda, N. 2001, *Astronomical Data Analysis Software and Systems X*, ed. F. R. Harnden, Jr., F. A. Primini, & H. E. Payne, 229
- Lupton, R. H., Gunn, J. E., & Szalay, A. S. 1999, *AJ*, 118, 1406
- Okamoto, T., & Nagashima, M. 2001, *ApJ*, 547, 109
- Paolillo, M., Andreon, S., Longo, G., Puddu, E., Gal., R. R., Scaramella R., Djorgovski, S. G., de Carvalho, R. 2001, *A&A*, 367, 59
- Phillipps, S., Driver, S. P., Couch, W. J., & Smith, R. M. 1998, *ApJ*, 498, L119
- Rakos, K. D., Schombert, J. M., Odell, A. P., & Steindling, S. 2000, *ApJ*, 540, 715
- Sandage, A., Binggeli, B., & Tammann, G. A. 1985, *AJ*, 90, 1759
- Scranton, R., Johnston, D., Dodelson, S., Frieman, J. A., Connolly, A., Eisenstein, D. J., Gunn, J. E., Hui, L., et al. 2002, submitted to *ApJ*.
- Shimasaku, K., Fukugita, M., Doi, M., Hamabe, M., Ichikawa, T., Okamura, S., Sekiguchi, M., Yasuda, N., et al. 2001, *AJ*, 122, 1238
- Smith, J. A., Tucker, D. L., Kent, S., Richmond, M. W., Fukugita, M., Ichikawa, T., Ichikawa, S., Jorgensen, A. M., et al. 2002, *AJ*, 123, 2121
- Springel, V., White, S. D. M., Tormen, G., & Kauffmann, G. 2001, *MNRAS*, 328, 726

- Stoughton, C., Lupton, R. H., Bernardi, M., Blanton, M. R., Burles, S., Castander, F. J., Connolly, A. J., Eisenstein, D. J., et al. 2002, *AJ*, 123, 485
- Strateva, I., Ivezić, Željko, Knapp, G. R., Narayanan, V. K., Strauss, M. A., Gunn, J. E., Lupton, R. H., Schlegel, D., et al. 2001, *AJ*, 122, 1861
- Struble, M. F., & Rood, H. J. 1987, *ApJ*, 323, 468
- Stoughton et al. 2002, accepted for *AJ*
- Trentham, N. 1998, *MNRAS*, 294, 193
- Valotto, C. A., Moore, B., & Lambas, D. G. 2001, *ApJ*, 546, 157.
- Valotto, C. A., Nicotra, M. A., Muriel, H., & Lambas, D. G. 1997, *ApJ*, 479, 90.
- Whitmore, B. C., Gilmore, D. M., & Jones, C. 1993, *ApJ*, 407, 489
- Yagi, M., Kashikawa, N., Sekiguchi, M., Doi, M., Yasuda, N., Shimasaku, K., & Okamura, S. 2002a, *AJ*, 123, 66
- Yagi, M., Kashikawa, N., Sekiguchi, M., Doi, M., Yasuda, N., Shimasaku, K., & Okamura, S. 2002b, *AJ*, 123, 87
- York, D. G., Adelman, J., Anderson, J. E., Anderson, S. F., Annis, J., Bahcall, N. A., Bakken, J. A., Barkhouser, R., et al. 2000, *AJ*, 120, 1579

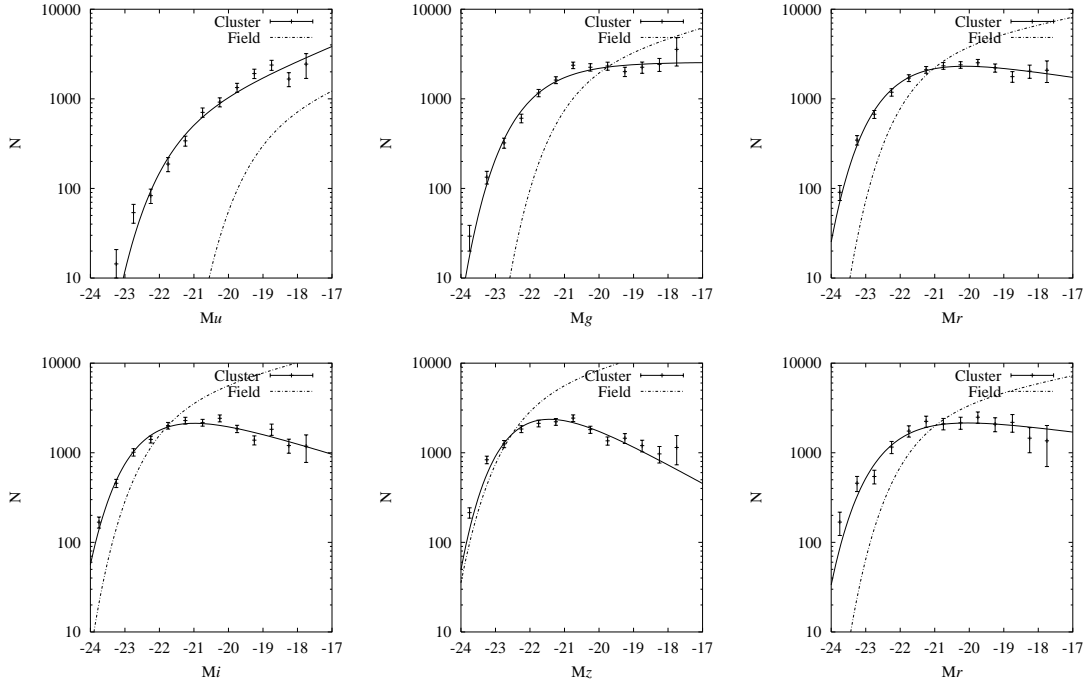


Fig. 1. Composite LF of galaxy clusters from the SDSS CE galaxy cluster catalog in five SDSS bands. The solid line is the best-fit Schechter functions. The y-axis is arbitrary. The dotted line is the field LFs from Blanton et al. (2001) re-scaled to our cosmology. The normalization of field LFs was adjusted to match the cluster best-fit Schechter functions. The lower-right panel is for clusters with spectroscopic redshifts in r . The best-fit Schechter parameters are summarized in table 1.

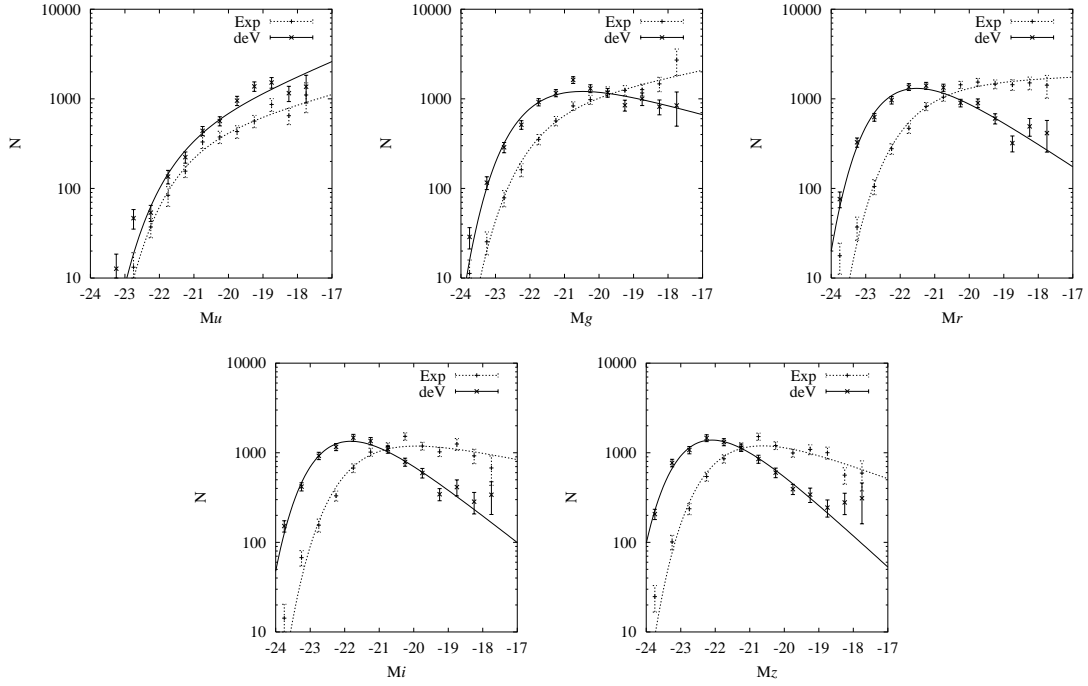


Fig. 2. Composite luminosity functions of de Vaucouleur galaxies and exponential galaxies. The galaxies are divided into two subsamples using profile fitting. The lines show the best-fit Schechter functions (solid for de Vaucouleur galaxies, dotted for exponential galaxies). The y-axis is arbitrary. de Vaucouleur galaxies always have a brighter M^* and a flatter faint end tail. The best-fit Schechter parameters are summarized in table 2.

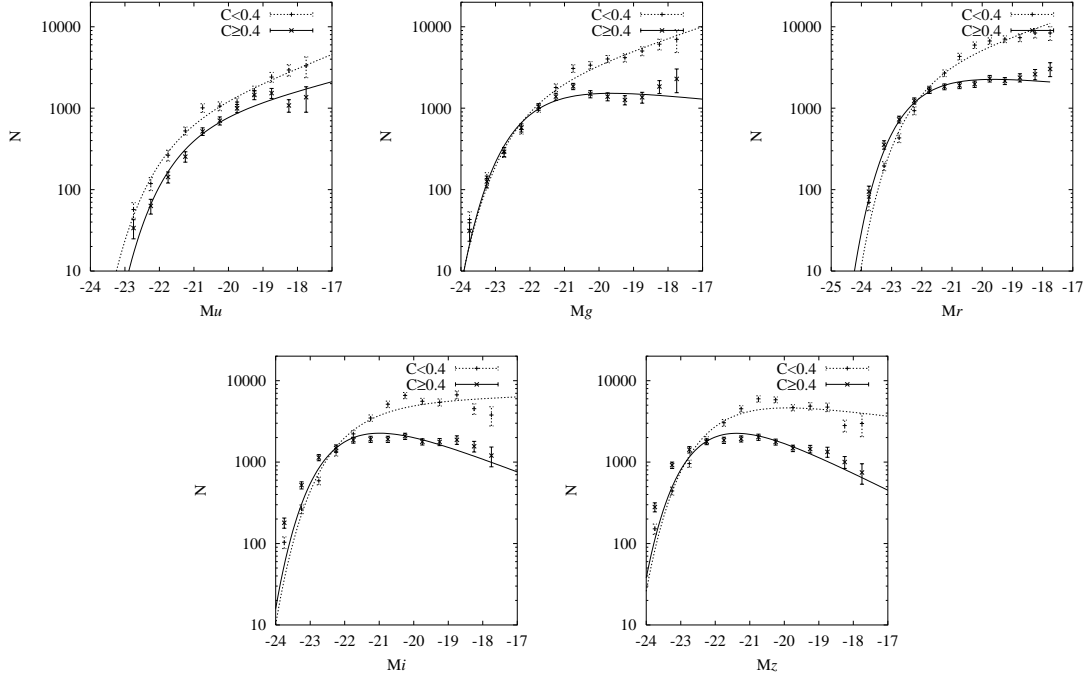


Fig. 3. Composite luminosity functions of high-concentration and low-concentration galaxies. The concentration index (C) used here is the ratio of the 50% Petrosian flux radius to the 90% Petrosian flux radius. In this figure, early-type galaxies have $C < 0.4$, and late-type galaxies have $C \geq 0.4$. Early-type galaxies have flatter faint end tails in all five bands. Lines are the best-fit Schechter functions (solid for $C < 0.4$, dotted for $C \geq 0.4$). The y-axis is arbitrary. The best-fit Schechter parameters are summarized in table 3.

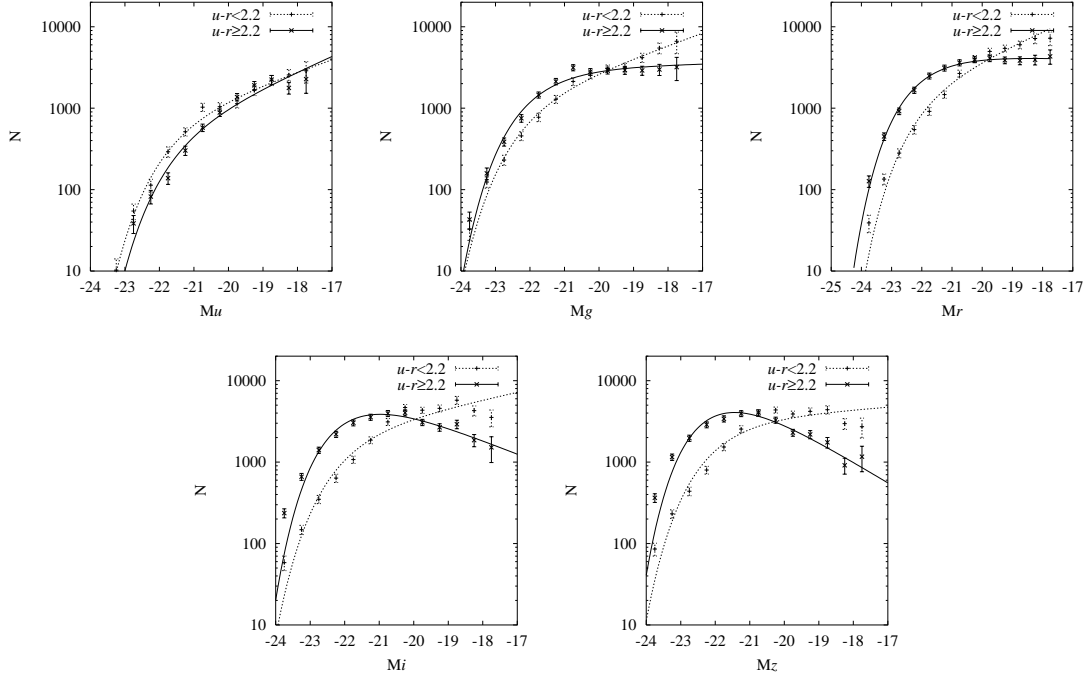


Fig. 4. Composite luminosity functions of $u - r < 2.2$ (late-type) and $u - r \geq 2.2$ (early-type) galaxies. Early-type galaxies have flatter faint end tails in all five bands. The lines are the best-fit Schechter functions (solid for $u - r < 2.2$, dotted for $u - r \geq 2.2$). The y-axis is arbitrary. The best-fit Schechter parameters are summarized in table 4.

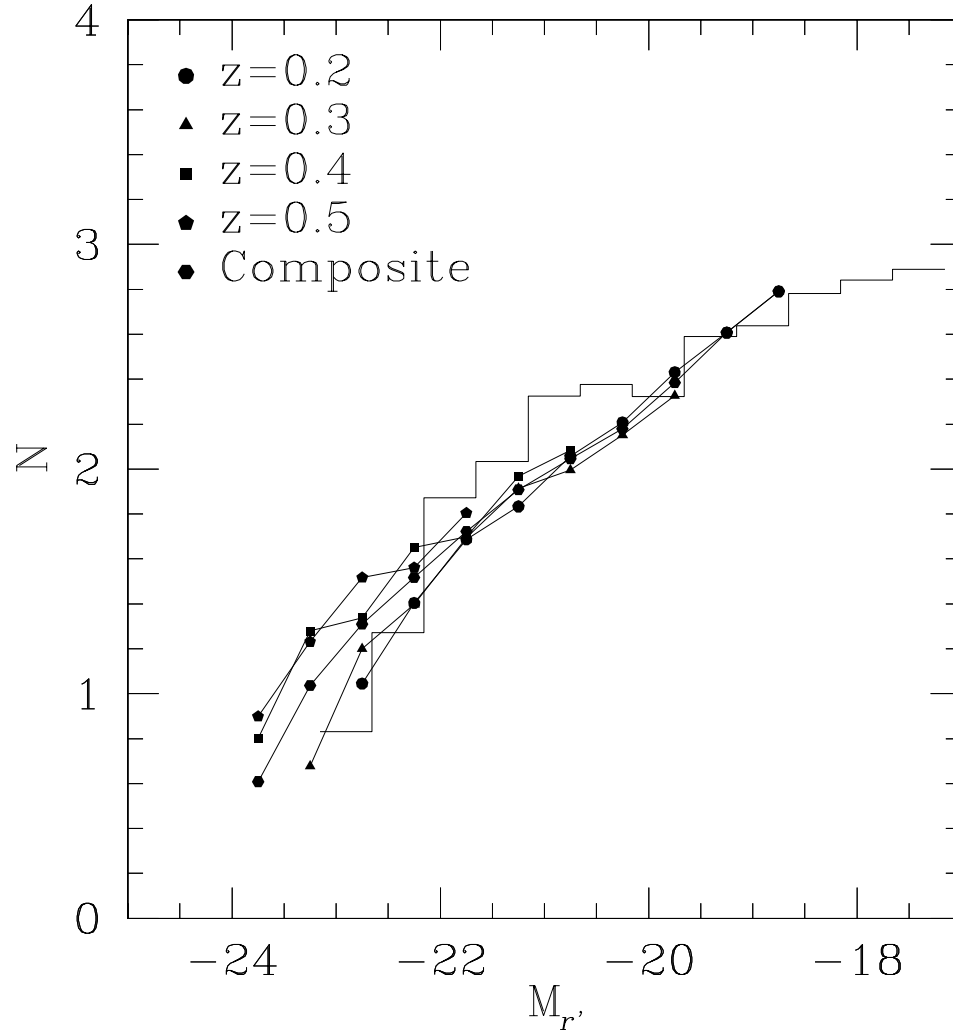


Fig. 5. Results of a Monte-Carlo simulation to test the robustness of the weighting scheme. The histogram shows the luminosity function of model cluster A 1577. The Circles, triangles, squares and pentagons represent the composite luminosity function at each redshift ($z = 0.2, 0.3, 0.4$ and 0.5 , respectively) constructed with 100 fake clusters at each redshift. The hexagonal points show the composite luminosity function from all 400 fake clusters distributed on the real SDSS data.

Table 1. Best-fit Schechter parameters of the composite luminosity function of five SDSS bands. The field values are from Blanton et al. (2001), whose parameters were shifted to match our cosmology. Galaxies within 0.75 Mpc are used.

Band	M^*	α	Field M^*	Field α
<i>u</i>	-21.61 ± 0.26	-1.40 ± 0.11	-19.11 ± 0.08	-1.35 ± 0.09
<i>g</i>	-22.01 ± 0.11	-1.00 ± 0.06	-20.81 ± 0.04	-1.26 ± 0.05
<i>r</i>	-22.21 ± 0.05	-0.85 ± 0.03	-21.60 ± 0.03	-1.20 ± 0.03
<i>i</i>	-22.31 ± 0.08	-0.70 ± 0.05	-22.03 ± 0.04	-1.25 ± 0.04
<i>z</i>	-22.36 ± 0.06	-0.58 ± 0.04	-22.32 ± 0.05	-1.24 ± 0.05
<i>r</i> (spec)	-22.31 ± 0.13	-0.88 ± 0.07

Table 2. Best-fit Schechter parameters for de Vaucouleur and exponential galaxies in five SDSS bands. The galaxies are divided into two subsamples using profile fitting. Galaxies within 0.75 Mpc are used.

Band	M^* (deV)	α (deV)	M^* (exp)	α (exp)
<i>u</i>	-21.64 ± 0.30	-1.41 ± 0.12	-21.45 ± 0.13	-1.27 ± 0.07
<i>g</i>	-21.92 ± 0.11	-0.73 ± 0.07	-21.89 ± 0.13	-1.20 ± 0.06
<i>r</i>	-22.01 ± 0.07	-0.37 ± 0.06	-21.73 ± 0.12	-1.04 ± 0.06
<i>i</i>	-22.13 ± 0.07	-0.25 ± 0.06	-21.69 ± 0.13	-0.80 ± 0.08
<i>z</i>	-22.24 ± 0.06	$+0.12 \pm 0.06$	-21.76 ± 0.11	-0.65 ± 0.07

Table 3. Best-fit Schechter parameters for low concentration (early-type) and high concentration (late-type) galaxies in five SDSS bands. The concentration index here is the ratio of 50% Petrosian flux radius to 90% Petrosian flux radius. Early-type galaxies have a concentration of <0.4 , and late-type galaxies have a concentration of ≥ 0.4 . Galaxies within 0.75 Mpc are used.

Band	M^* (Early)	α (Early)	M^* (Late)	α (Late)
<i>u</i>	-21.42 ± 0.24	-1.28 ± 0.12	-21.82 ± 0.11	-1.42 ± 0.06
<i>g</i>	-22.05 ± 0.11	-0.89 ± 0.07	-22.26 ± 0.11	-1.36 ± 0.05
<i>r</i>	-22.31 ± 0.06	-0.92 ± 0.04	-22.24 ± 0.12	-1.32 ± 0.06
<i>i</i>	-21.97 ± 0.09	-0.59 ± 0.10	-22.02 ± 0.13	-1.04 ± 0.08
<i>z</i>	-22.08 ± 0.09	-0.47 ± 0.09	-22.09 ± 0.12	-0.87 ± 0.07

Table 4. Best-fit Schechter parameters for $u-r > 2.2$ (early type) and $u-r \leq 2.2$ (late type) galaxies in five SDSS bands. Galaxies within 0.75 Mpc are used.

Band	M^* (Early)	α (Early)	M^* (Late)	α (Late)
<i>u</i>	-21.65 ± 0.26	-1.47 ± 0.11	-21.78 ± 0.13	-1.37 ± 0.07
<i>g</i>	-22.04 ± 0.10	-1.03 ± 0.06	-22.30 ± 0.09	-1.38 ± 0.05
<i>r</i>	-22.29 ± 0.04	-0.97 ± 0.02	-22.22 ± 0.12	-1.41 ± 0.06
<i>i</i>	-21.91 ± 0.08	-0.58 ± 0.07	-22.17 ± 0.16	-1.23 ± 0.08
<i>z</i>	-21.93 ± 0.07	-0.36 ± 0.08	-22.14 ± 0.19	-1.08 ± 0.09

Table 5. Best-fit Schechter parameters for galaxies using positions of brightest cluster galaxies as a center in five SDSS bands. The mean deviation from the CE center used in this work is 1.02 arcmin.

Band	M^*	α
<i>u</i>	-21.84 ± 0.16	-1.43 ± 0.07
<i>g</i>	-22.16 ± 0.15	-1.05 ± 0.07
<i>r</i>	-22.29 ± 0.05	-0.91 ± 0.03
<i>i</i>	-22.31 ± 0.06	-0.73 ± 0.03
<i>z</i>	-22.18 ± 0.07	-0.55 ± 0.07

Table 6. Best-fit Schechter parameters for galaxies using global background subtraction in five SDSS bands. Instead of the annuli around the cluster, the global background was used to subtract the background galaxies to see the dependence on the background subtraction.

Band	M^*	α
<i>u</i>	-21.77 ± 0.17	-1.47 ± 0.07
<i>g</i>	-22.01 ± 0.12	-1.06 ± 0.07
<i>r</i>	-22.20 ± 0.05	-0.90 ± 0.03
<i>i</i>	-22.24 ± 0.07	-0.72 ± 0.04
<i>z</i>	-22.10 ± 0.06	-0.50 ± 0.06

Table 7. Best-fit Schechter parameters in the *r* band for galaxies using richer systems. The best-fit Schechter parameters for $N_{-18} > 20$ and $N_{-18} > 40$ subsamples are shown. N_{-18} is defined as the number of galaxies brighter than -18 th magnitude after subtracting the background.

Band	M^*	α	$N(\text{cluster})$
$N_{-18} > 20$	-22.21 ± 0.05	-0.85 ± 0.03	204
$N_{-18} > 40$	-22.29 ± 0.06	-0.90 ± 0.04	120

Table 8. Comparison with previous studies on the composite luminosity function. The CE composite LFs (this work) was re-calculated using each author’s cosmology. The magnitude was transformed using data from Fukugita et al. (1995) and Lumsden et al. (1992).

Paper	M^*	α	Band	Ncluster	Cosmology
CE	-22.21 ± 0.05	-0.85 ± 0.03	r	204	$\Omega_M=0.3 \Omega_\Lambda=0.7 H_0=70$
Colless 89	-20.04	-1.21	bj	14 rich	$H_0=100 q_0=1$
(CE)	-21.58 ± 0.12	-0.93 ± 0.06	bj	204	$H_0=100 q_0=1$
(CE)	-22.20 ± 0.12	-1.21 fixed	bj	204	$H_0=100 q_0=1$
Lugger 89	-22.81 ± 0.13	-1.21 ± 0.09	R (PDS)	9	$H_0=50$
(CE)	-22.49 ± 0.06	-0.69 ± 0.05	R (PDS)	204	$H_0=50 q_0=0.5$
(CE)	-22.77 ± 0.17	-1.21 fixed	R (PDS)	204	$H_0=50 q_0=0.5$
Valotto 97	-20.0 ± 0.1	-1.4 ± 0.1	bj	55 Abell APM	$H_0=100$
(CE)	-21.58 ± 0.12	-0.93 ± 0.06	bj	204	$H_0=100 q_0=1$
(CE)	-22.69 ± 0.23	-1.4 fixed	bj	204	$H_0=100 q_0=1$
Lumsden 97	-20.16 ± 0.02	-1.22 ± 0.04	bj	22 rich	$H_0=100 q_0=1$
(CE)	-21.58 ± 0.12	-0.93 ± 0.06	bj	204	$H_0=100 q_0=1$
(CE)	-22.22 ± 0.10	-1.22 fixed	bj	204	$H_0=100 q_0=1$
Garilli 99	-22.16 ± 0.15	-0.95 ± 0.07	r (CCD)	65 Abell X-ray	$H_0=50 q_0=0.5$
(CE)	-22.15 ± 0.06	-0.69 ± 0.05	r (CCD)	204	$H_0=50 q_0=0.5$
(CE)	-22.28 ± 0.05	-0.84 fixed	r (CCD)	204	$H_0=50 q_0=0.5$
Paolillo 00	-22.26 ± 0.16	-1.11	r (POSSII)	39 Abell	$H_0=50 q_0=0.5$
(CE)	-22.15 ± 0.06	-0.69 ± 0.05	r (POSSII)	204	$H_0=50 q_0=0.5$
(CE)	-22.55 ± 0.12	-1.11 fixed	r (POSSII)	204	$H_0=50 q_0=0.5$
Yagi 02	-21.3 ± 0.2	-1.31 ± 0.05	R_C	10 Abell	$H_0=100 q_0=0.5$
(CE)	-21.89 ± 0.10	-1.03 ± 0.05	R_C	204	$H_0=100 q_0=0.5$
(CE)	-22.55 ± 0.14	-1.31 fixed	R_C	204	$H_0=100 q_0=0.5$